J4.8 VERY HIGH RESOLUTION PRECIPITATION FORECASTING ON LOW COST HIGH PERFORMANCE COMPUTER SYSTEMS IN SUPPORT OF HYDROLOGICAL MODELING

Daniel Soderman[1], Francesco Meneguzzo[2*], Bernardo Gozzini[2], Daniele Grifoni[2], Gianni Messeri[3], Matteo Rossi[3], Simone Montagnani[3], Massimiliano Pasqui[2], Andrea Orlandi[2], Alberto Ortolani[3], Ezio Todini[4], Giovanni Menduni[5], and Vincenzo Levizzani[6]

[1]Foreca Ltd, Pursimiehenkatu 29-31B, 00150 Helsinki, Finland
[2]Institute of Biometeorology - National Research Council (IBIMET-CNR), Firenze, Italy
[3]Laboratory for Meteorology and Environmental Modeling (LaMMA-Regione Toscana), Firenze, Italy
[4]Department of Earth and Geo-Environmental Sciences, University of Bologna, Bologna, Italy
[5]Arno River Basin Authority, Firenze, Italy
[6] Institute of Atmospheric Sciences and Climate - National Research Council (ISAC-CNR), Bologna, Italy

1. INTRODUCTION

Early flash flood warnings are needed to improve the effectiveness of civil protection efforts to mitigate damages and save lives. This is especially true for small to medium size (sub-) basins where the response times to rainfall input are of the order few hours or less.

This is the case of the Arno River Basin (Italy), and of virtually any basin, when upper sections are considered.

As part of the effort to produce continuous accurate hydrological flood forecasts along the Arno river and its tributaries, the Arno River Basin Authority sponsors the verification and improvement of the operational Regional Atmospheric Modeling System (RAMS) as an effective QPF tool to feed hydrological (flood) models in the frame of the ARTU project (http://www.arno.autoritadibacino.it).

Furthermore, the EURAINSAT project (an EC research project co-funded by the Energy, Environment and Sustainable Development Programme within the topic "Development of generic Earth observation technologies", Contract number EVG1-2000-00030) sponsors the development of the RAMS model with the twofold purpose of providing reliable input to rapid update satellite precipitation estimation algorithms and using such estimates to effectively improve mesoscale QPF forecasts by means of operational precipitation assimilation (http://www.isac.cnr.it/~eurainsat).

Finally, the MUSIC project (research project also co-funded by the EC under the above Development Programme within the topic "Development of generic Earth observation technologies", Contract number EVK1-CT-2000-00058) sponsors the development of advanced hydro-meteorological forecasting tools, where accurate QPF plays a decisive role.

The need to run the RAMS model over different domains at varying horizontal resolutions led to the use of low cost high performance and effectively scaling computer systems.

2. THE RAMS MODEL

The Regional Atmospheric Modeling System, RAMS, version 4.4, is used for the operational mesoscale weather forecasts at the Regional Meteorological Service of Tuscany, Italy (Meneguzzo et al., 2002; see also: http://www.lamma.rete.toscana.it/rams-web/e_index.html), and was used for all the case studies described in the following.

RAMS was originally developed in the early 70's essentially as a research tool; now it is widely used both for research and operational forecast purposes in many operational centers around the world. Since the early '90s a large number of improvements have been introduced both as regards the physics (mainly moist and land surface processes) and the computational point design (new numerical schemes and parallel computing). A general description of the model can be found in Pielke et al. (1992), while a technical description can be found in MRC/*Aster (2000).

RAMS today represents the state-of-the-art in atmospheric numerical modeling being continuously improved on the basis of multi-disciplinary work both at Colorado State

* *Corresponding author address:* Francesco Meneguzzo, Institute of Biometeorology, National research Council, Via Caproni 8, 50145 Firenze, Italy; e-mail: meneguzzo@lamma.rete.toscana.it

University and at several other research and operational centers worldwide. Beyond numerical modelers, meteorologists, computer experts, remote sensing experts, geographers, agronomists, forest experts and geologists participate to the development of the various of components of RAMS.

2.1 Initialization; objective analysis

RAMS needs a set of atmospheric data analyzed over the domain grid and at its boundaries both at the initial time of the simulation and at future times. Several data types can be combined and processed by an isentropic analysis package (ISAN). The isentropic coordinates have several advantages as regards to other coordinate systems: since the synoptic scale atmospheric flow is to a first approximation adiabatic, the objective analysis performed over an isentropic surface will "pack" in frontal areas, thus providing a higher resolution description of the discontinuities.

Besides, since the isentropic surfaces are steeper close to the fronts, shorter wavelength features are transformed into longer wavelength ones and can be analyzed more accurately. ISAN allows a separate data analysis over the different nested grids (two-way nesting is implemented), thus leading to a better use of data from dense networks. The atmospheric fields distributed over regular grids which are generally provided by larger scale models, are first analyzed and interpolated over the RAMS grid using a polar-stereographic domain which minimizes distortions. Following, the data are vertically interpolated in the isentropic and terrain-following co-ordinate systems. After this, a large set of a variety of data types can be assimilated.

The Barnes (1973) objective analysis scheme is used for wind, pressure and relative humidity. The local surface observation data over land and water can be assimilated and propagated along the vertical up to a variable altitude. A four-dimensional data assimilation scheme has been implemented in RAMS, where the model fields can be nudged towards the observations during the simulations; a further nudging term is thus added to the prognostic equations.

2.2 Basic Equations

The basic equations of RAMS are three dimensional, non-hydrostatic, compressible and time-split in an horizontal rotated polar-stereographic transformation and vertical terrain following height. The non-hydrostatic formulation and the large number of terms retained in the RAMS equations allow to attain in principle any spatial horizontal resolution, which has made applications from planetary climate to tunnel wind possible.

2.3 Microphysics

The representation of cloud and precipitation microphysics in RAMS includes the treatment of each water species (cloud water, rain, pristine ice, snow, aggregates, graupel, hail) as a generalized Gamma distribution (Pielke et al., 1992; Walko et al., 1995). The scheme allows hail to contain liquid water and contains the description of the homogeneous and heterogeneous ice nucleation, and the ice size change by means of vapor deposition and sublimation.

A very efficient solution technique is available for the stochastic collection equation and a new technique for the prediction of sedimentation or precipitation of hydrometeors, allowing the definition of the fall velocity on the basis of the gamma size distribution.

2.4 Representation of Cumulus Convection

The cumulus convection parameterization in RAMS (Tremback, 1990), which is still to be applied to coarse grids (over 15 km horizontal spatial resolution) is relatively simple. This reflects on one side the greater effort spent towards the explicit representation of convective processes at very high resolution, and on the other the consideration that simple cumulus convection schemes allow more straightforward assimilation of non standard data such as cloud and precipitation observations (diabatic initialization).

The scheme implemented in RAMS is a generalized form (Molinari, 1995; Molinari et al., 1995) of the Kuo (1974) equilibrium scheme.

The equilibrium schemes assume that the convection is fed by the consumption of the conditional instability, with a speed equal to its production by the processes occurring at the grid mesh size scale.

Convection can be generated by a large number of different causes, the main of which is represented by the low level air mass convergence originated by gravity waves, where its interaction with the boundary layer sometimes can trigger the convection.

The cumulus convection schemes deal with the convection dynamics as a sub-grid process, i.e. not explicitly solved by the equations of motion.

This imposes a lower limit to the model resolution enhancement, since at high resolutions a convective process might span more grid nodes, thus undermining the sub-grid hypothesis.

2.5 Representation of Land Surface Processes

The surface heterogeneities connected to the vegetation cover and the land use are assimilated and represented in great detail in RAMS by means of the LEAF-2 (Land Ecosystem Atmosphere Feedback) model.

LEAF-2 (Walko et al., 2000) represents the vertical exchange of water and heat in several soil layers, including the effects of freezing and melting, the temporary water and snow cover, the vegetation and the canopy air. The surface domain meshes are further sub-divided into patches, each identified by a separate vegetation cover and land use, soil type and initial soil moisture (Fig. 1).

The balance equations for soil energy and moisture, surface water, vegetation and canopy air, and exchange with the free atmosphere, are solved separately for each patch. A hydrological model based on the Darcy law for the lateral downslope water transport exchanges the moisture in the sub-surface saturated layers and the surface runoff.

LEAF-2 assimilates standard land use datasets to define the prevailing land cover in each grid mesh and possibly the patches, then parameterizes the vegetation effects by means of biophysical quantities.

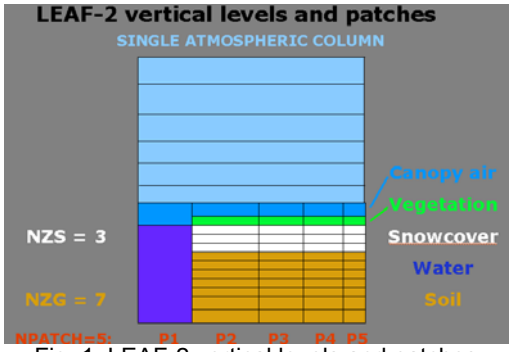

Fig. 1. LEAF-2 vertical levels and patches

3. COMPUTATIONAL SYSTEM AND COMPUTING PERFORMANCES

Numerical weather prediction models are amongst the computationally most demanding systems in existence so far. Using a complete set of Navier – Stokes equations along with complexes numerical schemes for soil – vegetation – air interactions and microphysical precipitation description enlarge the NWP computational demands. However, since few years, parallel computational systems based on the Linux operating system are becoming popular and today represent real "high performance – low cost" systems. Such parallel architectures also represent an alternative to massive parallel systems which are characterized by very high costs. The fundamental scheme is called Beowulf – like and it comprises a number of PCs, called also Nodes, connected through a switch together within a local area network (see scheme in Fig. 2).

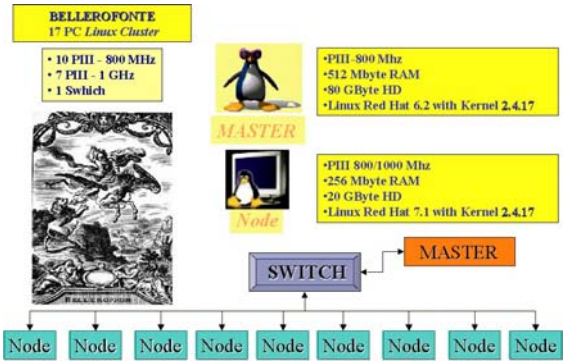

Fig. 2. Summary scheme of the Linux Beowulf Cluster, called "Bellerophon", used in this study

A special node, called "master" is the Dynamical Name Server and provides all the network specifics. A collection of libraries called "middleware" handles communicating and transferring information among nodes (Fig. 3).

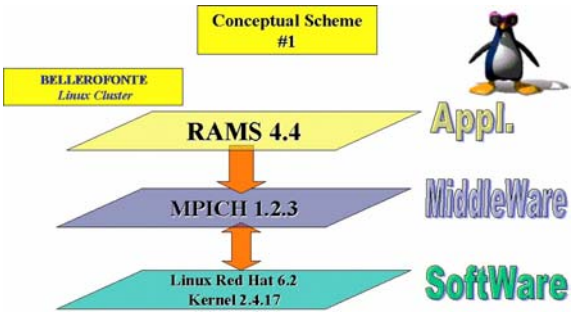

Fig. 3. Conceptual scheme of parallel computing by the use of a Linux Beowulf Cluster, where RAMS 4.4 is the Numerical Weather Model, MPICH stands for "Message Passing Interface Chamaleont", i.e. the actual parallel environment

Thus the number of operations needed, during an atmospheric simulation, is distributed among available cluster nodes reducing the total amount of overall time needed. A large number of problems arise, essentially due to the communication aspects between nodes. Network traffic, calibration and synchronicity among available nodes can reduce parallel computational efficiency, but essentially due both to the increased CPU computational power and to the availability of efficient and robust network drivers it is possible to achieve a good performance. Every simulation step is executed in a specific amount of seconds which is called

"Wall Clock Time" and depends on the computational system used.

Such time is the total time spent by the system to handle both computational and Input/Output data transfer, represented for example by the ingestion of boundary conditions and/or output data file production. Such activities, even though much longer, are less frequent than the pure computational ones, and represent a minor fraction of overall simulation time. As regards the specific RAMS behavior all the Input/Output transfer and computational job distribution is performed by the special node called "master" which doesn't play any actual computational role and which uses only a fraction of the Wall Clock Time. Table 1 summarizes the typical values for a medium size RAMS simulation.

Master Time	Wall Clock Time
Mean [s]	Mean [s]
0.19	6.00
Max. Value [s]	Max. Value [s]
7.93	24.47
Min. Value [s]	Min. Value [s]
0.05	5.03
Standard dev. [s]	Standard dev. [s]
0.88	1.20
Tot Time [h]	Tot Time [h]
0.22	7.17

Table 1. Summary table of time statistics both for Master process Time and Wall Clock Time

Typical performance values are presented in three graphs, including the Wall Clock Time series (Fig. 4), Master – process Wall Clock Time distribution (Fig. 5) and Node – process distribution an(Fig. 6).

In Fig. 4 a sequence of time steps is presented, where several regimes should be recognized due to different computational activities. In this case the I/O time step duration is essentially linked to the hourly model output frequency, and, during the first period, the larger amount of time needed is due to the other Linux System activities not connected with the simulation.

Analysis of the time step distribution reveals the small spread around the average values for the Master time step and the Wall Clock Time step as well (Figs. 5 and 6).

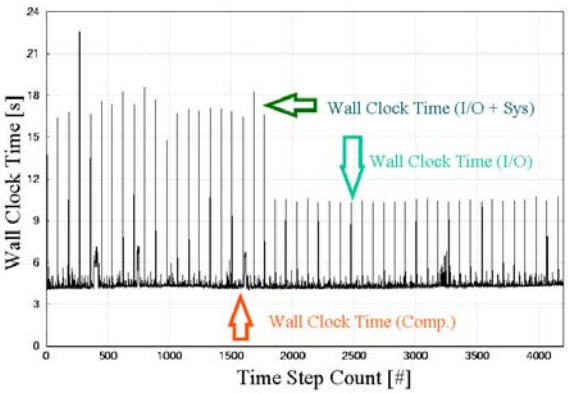

Fig. 4. Wall clock time series for a typical simulation, the total amount of time needed during a simulation time step could be divided into three different classes: computational (Comp), Input/Output data transfer (I/O), Linux operating system activities (Sys)

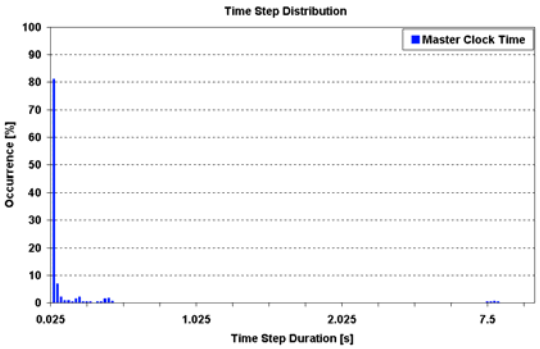

Fig. 5. Master time step distribution according to their duration in seconds

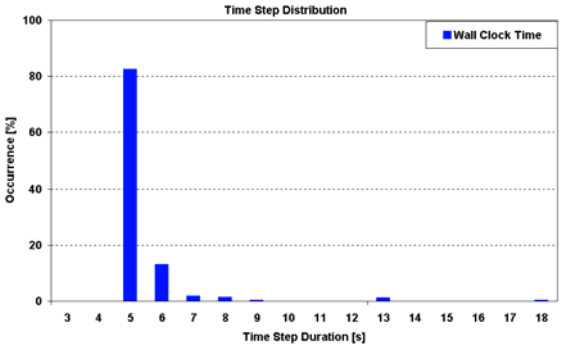

Fig. 6. Wall Clock Time distribution for each simulation step according to their duration in seconds

4. CASE STUDIES

4.1 Data and Methods

The RAMS model is used for mesoscale high-resolution atmospheric prediction in the Mediterranean area. The NCEP/NCAR reanalyses (Kalnay et al., 1996) provide its initialization for the historical floods which affected the Arno river (geography in Fig. 7).

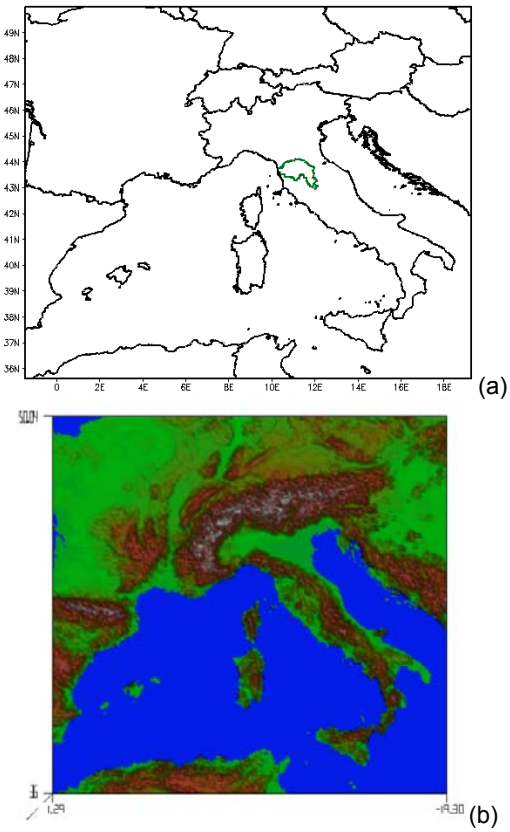

Fig. 7. Location of the Arno basin (dark green boundaries) in Europe (a) and orography of the same area (b)

The validation of RAMS forecasts, limited to precipitation (QPF), is also performed over relevant sub-basins of the Arno river (Fig. 8).

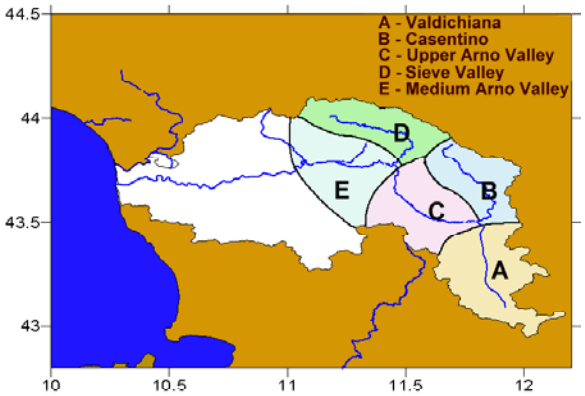

Fig. 8. Relevant sub-basins of the Arno River basin, where specific model validation was performed. Degrees are Latitude (positive north) and Longitude (positive east)

The ECMWF operational analyses provided the initialization for the MAP IOP2 case study chosen to demonstrate the performance of satellite precipitation assimilation.

4.2 ARTU and MUSIC Projects: Predicting Floods Affecting the Arno River

4.2.1 The hydrological model TOPKAPI

Rainfall-runoff models constitute the core of most flood forecasting systems, and whilst it is true that several new models have been developed in the last decades, it has been demonstrated that, for the purposes of flood forecasting, the most important effect they must represent is the dynamics of the overall soil filling and depletion mechanisms and the resulting variation in the size of the saturated basin area; in fact, when large portions of the basin reach saturation the rainfall that falls on the catchment has a direct effect on the flood magnitude without being attenuated by the soil's absorption capacity. These concepts have spawned models which are very widely used today and have been extensively described in the literature, such as the model developed by Zhao R.J., (1977), by Moore and Clarke (1981), the TOPMODEL (Beven and Kirkby, 1979) the ARNO (Todini, 1996).

More recently a new rainfall-runoff modelling approach, the TOPKAPI (TOPographic Kinematic APproximation and Integration) has been introduced (Ciarapica and Todini, 2002; Todini and Ciarapica, 2002), starting from a kinematic wave point representation of the movement of water in the soil and on the surface (Todini,1995). By integrating the point differential equations over the finite dimension of a pixel a non-linear reservoir model equation is obtained. The catchment behaviour can thus be reproduced by three cascades of non-linear reservoirs representing respectively, the soil, the surface, the drainage network.

The advantage of using distributed models, as TOPKAPI lies in the possibility of incorporating all the Digital Elevation Model (DEM) information and using appropriate soil and surface equations. Moreover, this type of physically based distributed model is definitely superior, due to the extremely reduced need for calibration and to the semi-distributed conceptual models, such as Sacramento (Burnash, 1973) or SSAR (Rockwood, 1961; Rockwood and Nelson, 1966; Rockwood *et al*, 1972) or ARNO (Todini, 1996), which have been widely used in the past for developing real time flood forecasting systems.

TOPKAPI does not require the classical calibration: parameters such as porosity and hydraulic conductivity can be established on the basis of the soil types and land use, while roughness for the overland flow can be related to the land use and the roughness in the

drainage network can be related to the order of the channel in the drainage system.

Finally, as opposed to Shetran or Mike She (Abbott et al, 1986a,b) which require long computational time, TOPKAPI runs very fast, since its equations are solved analytically and the speed of computation makes it compatible with operational real time flood forecasting. For instance, in the model of the Arno river, where three cascades of approximately 8000 non-linear reservoirs are solved at each time step, therefore, the computation of discharges for one full year at hourly time steps requires only 8 minutes on a standard PC.

Several applications of TOPKAPI have been completed chiefly for the development of real time flood forecasting systems: the following two applications highlight the interesting properties of the model in the case of a relatively small catchment with data available from a dense rain gauge tele-metering network, and in the case of a very large one using free of charge data available on the web.

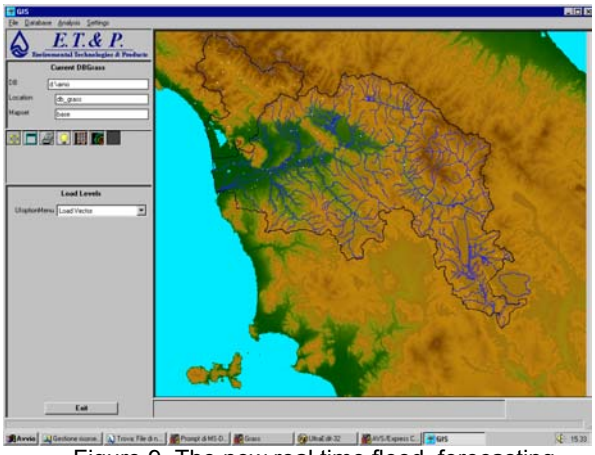

Figure 9. The new real time flood forecasting system for the Arno

The application of TOPKAPI to the Arno river aimed at forecasting floods at Florence (the Nave di Rosano gauging station is just upstream Florence) using 1 by 1 km pixels. Fig. 9 shows the front end of the operational real time flood forecasting system developed on the Arno river.

No calibration was applied and the model parameter values were derived from literature. The drainage network was derived from the Digital Elevation Model available through HYDRO1K of USGS (Fig. 10); soil parameters were estimated from tables provided by the USDA on the basis of soil types (Fig. 11) and land use (Fig. 12) maps; overland and channel roughness values were derived from Chow (1959) and from Barnes (1967) according to land use and channel order.

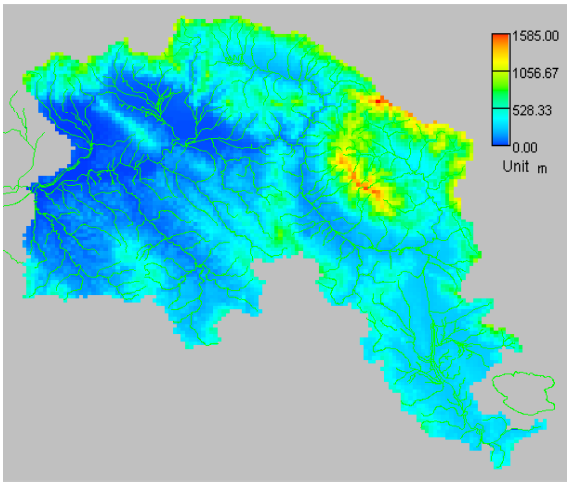

Figure 10. The 1x1 km Digital Elevation Model of the Arno basin

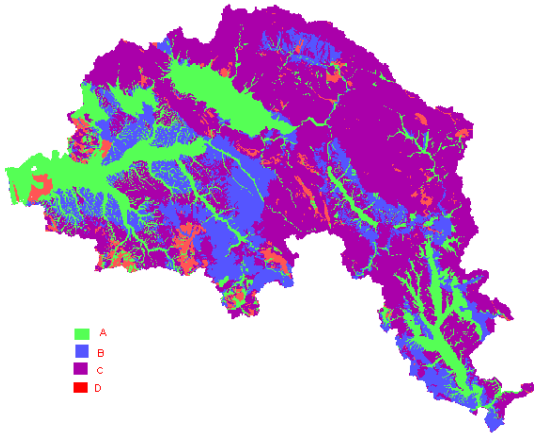

Figure 11. The soil types map for the Arno River

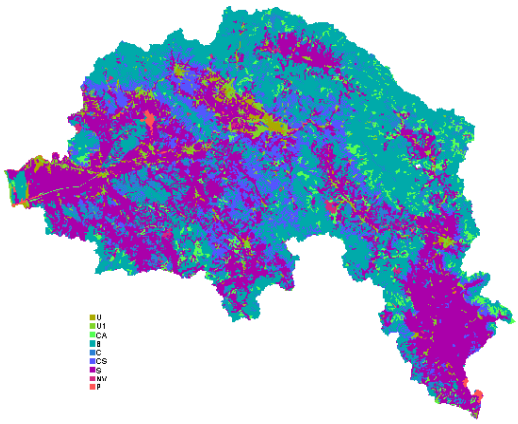

Figure 12. The land use map for the Arno basin (from Corine)

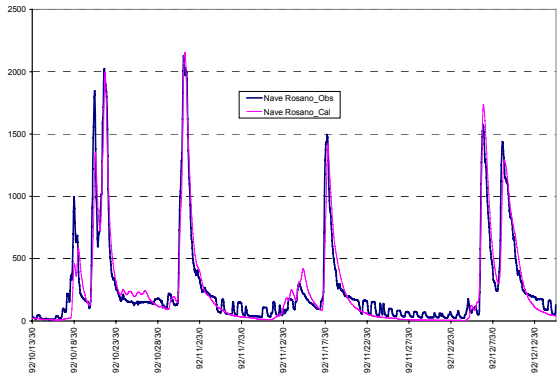

Figure 13. Calibration results at Nave di Rosano, immediately upstream Florence

Although numerical measures of fit tests are available, as one can understand from Fig. 13, calibration of the TOPKAPI model was considered successful and appropriate for real-time flood forecasting on the Arno basin.

4.2.2 100-year flood: November 1966

At 00 UTC on November 2, 1966 a high-pressure belt extended over a great part of the Atlantic Ocean, the British Isles, Scandinavia, and east to Russia (peak pressure of 1044 hPa).

Over central-southern Europe a low pressure field dominated, with a relatively organized structure over the Gulf of Biscay. The main cyclonic westerlies over the Atlantic were temporarily confined to far northern latitudes. In the mid-troposphere a wide through extended from Scandinavia to the Iberian Peninsula, associated with very cold air masses, a distinct cold advection over the Mediterranean, and a high-troposphere jet followed the tightest isobars. Notable is the great wave amplitude, about 40° latitude.

On November 3 the situation evolved to greater vorticity in the through, also as a consequence of the vorticity advection by the jet stream from very northern latitudes, and the deepening of the surface vortex. The through axis started rotating anti-clockwise, triggering a strong elevated heat wave over central Mediterranean and a dynamic ridge over Balkans and eastern Europe. Ascending vertical velocity also developed west of Italy.

At 00 UTC on November 4, the north Atlantic very cold air masses reached western Mediterranean, feeding the (deepening) cyclonic vortex over central-western Mediterranean with extreme baroclinic instability. The heat flux over eastern Italy and further east reinforced, leading to surface jets and a sudden geopotential increase. A blocking situation rapidly developed (1032 hPa peak pressure over Balkans). Extreme ascending vertical velocity was found over western and northern Italy.

Starting from early afternoon on November 4, the surface low weakened after the baroclinic instability flux diminished. Thermal advection rapidly weakened too, and an elevated weak ridge grew over western Mediterranean. Vertical velocity changed sign over western Italy during November 4.
Such evolution is synthetically described in Fig. 14.

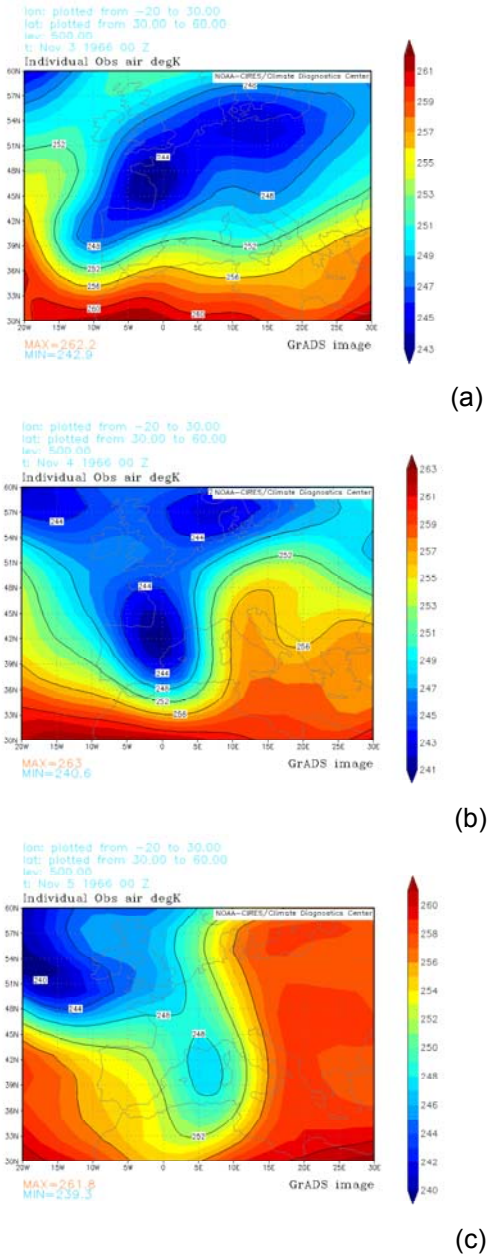

Figure 14. 500-hPa geopotential heights at 00 UTC on November 3 (a), November 4 (b) and November 5 (c), 1966

The precipitation which fell during the event was absolutely extreme, reaching more than 300 mm in Tuscany (central-western Italy) and more than 500 mm in north-eastern Italy. The rain volumes were also extraordinary.

Over the Arno basin, the highest precipitation fell during November 3, afternoon,

and cumulated precipitation averaged to about 120 mm in the period 12 UTC November 3 to 12 UTC November 4 (Fig. 15).

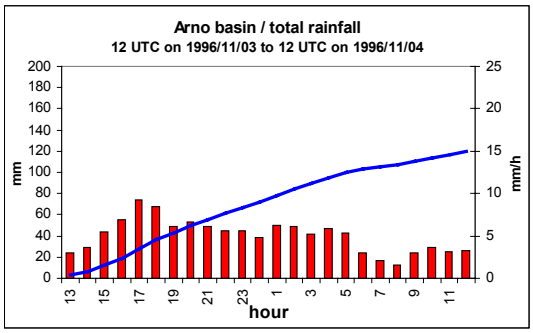

Figure 15. Average precipitation over the Arno river basin (hourly and cumulated)

Four simulations were executed, each one with three to four nested grids (two-ways nesting), and 26, 36 and 50 vertical levels. The relevant features are explained in Table 2. below.

NAME	START	DURATION	HORIZONTAL RESOLUTION				VERTICAL LEVELS
			G 1	G 2	G 3	G 4	
LIV36Ini12	3 NOV / 12 UTC	36 hours	80	16	3.2		36
LIV36Ini12G4	3 NOV / 12 UTC	36 hours	80	16	3.2	1.6	36
LIV50Ini12	3 NOV / 12 UTC	36 hours	80	16	3.2		50
LIV26Ini12	3 NOV / 12 UTC	36 hours	80	16	3.2		26

Table 2. Summary of features of the four RAMS simulations for the November 1966 flood

The three/four RAMS' grids are shown in Fig. 16. The vertical structures of the domains are shown in Fig. 17.

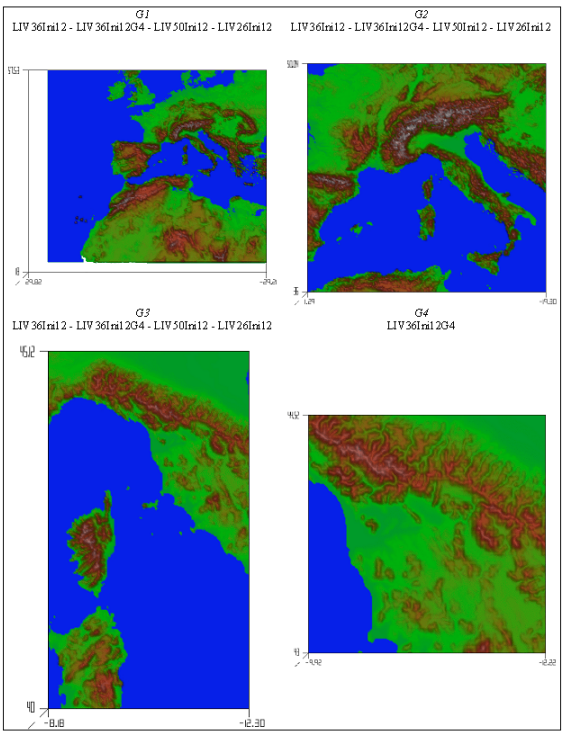

Figure 16. Horizontal domains of the RAMS simulations of the November 1966 flood

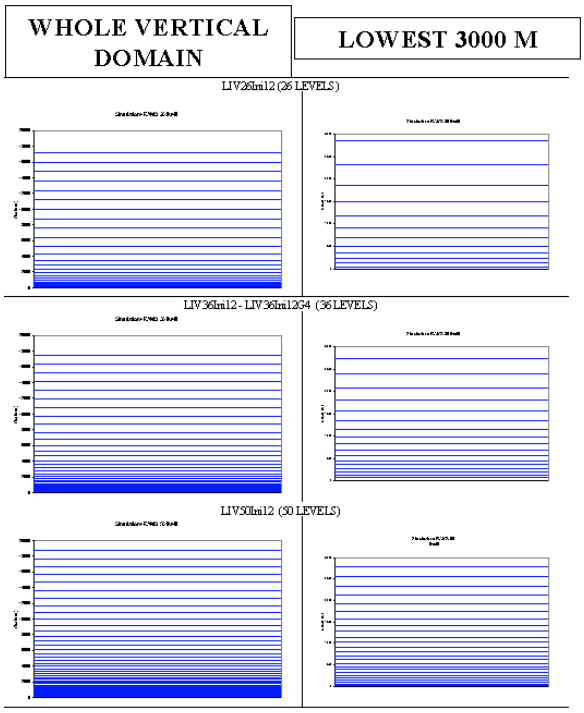

Figure 17. Vertical domains of the RAMS simulations of the November 1966 flood

The comparison of observed and predicted precipitation on the finest resolution grids for every simulation, in the period from 12 UTC on November 3rd to 12 UTC on November 4th are shown in Fig. 18 (patterns), Fig. 19 (basins averages), Fig. 20 (frequency in

intensity classes), Fig. 21 (Heidke Skill Score, e.g. Wilks, 1995).

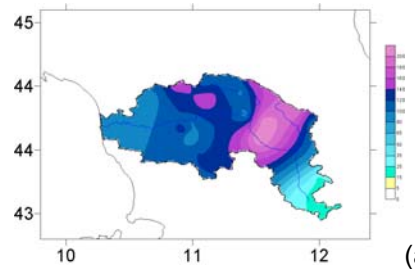

(a)

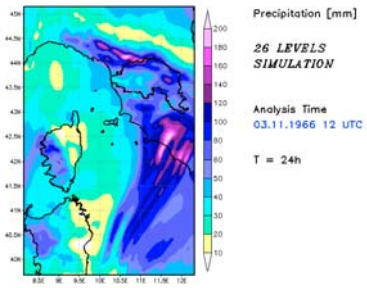

(b)

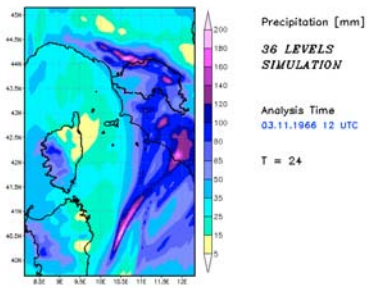

(c)

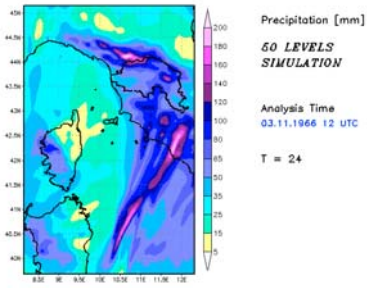

(d)

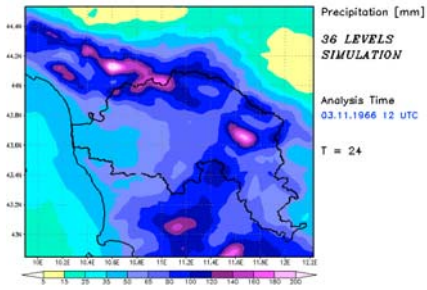

(e)

Figure 18. Validation of RAMS QPFs: comparison of observed vs forecast rainfall distributions. (a) Observations; (b) Liv26Ini12; (c) Liv36Ini12; (d) Liv50Ini12; (e) Liv36Ini12G4 (see Table 2)

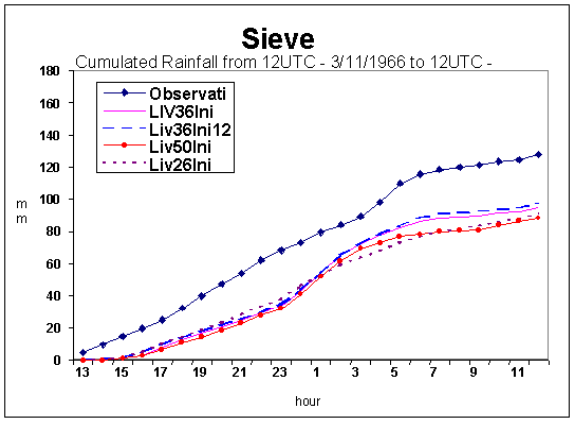

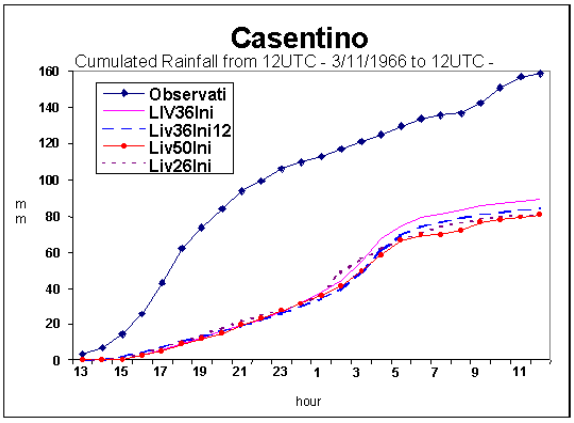

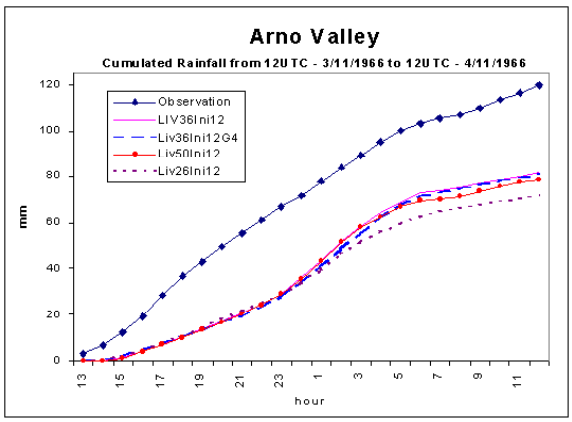

Figure 19. Validation of RAMS QPFs: comparison of observed vs forecast average rainfall over Sieve and Casrntino sub-basins and whole Arno watershed

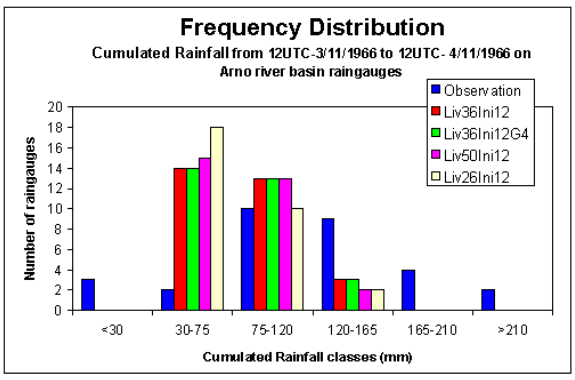

Figure 20. Validation of RAMS QPFs over the whole Arno watershed: comparison of observed vs forecast distribution of rainfall, partitioned into intensity classes

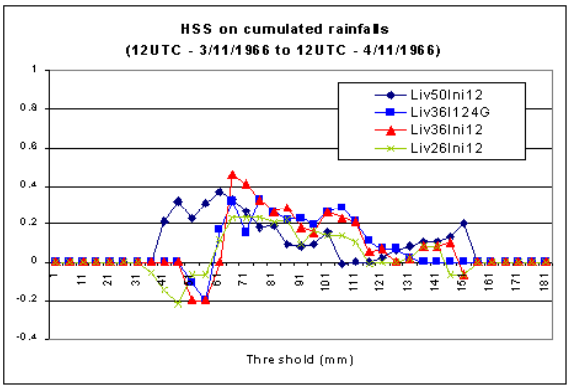

Figure 21. Validation of RAMS QPFs: Heidke Skill Score (HSS) of RAMS' QPFs

The validation vs the rain gauges provides some guidance to produce accurate QPFs:

- the event was a large scale one, spanning the Atlantic, central/western Europe, Mediterranean and northern Africa, and the precipitation systems covered hundreds of km;
- the resolution increase (3.2 km to 1.6 km) produces little effect, if any;
- the increase of vertical levels (and resolution) from 26 to 36 and, to a lesser extent, to 50 (which avoids some under-estimations), produces a very significant and sometimes decisive QPF improvement;
- under-estimation is apparent, anyway most of missing rainfall occurred in the early simulation period (model spin-up), suggesting that initial conditions and initialization time are relevant, and maybe that frequent runs are suitable for accurate QPF.

The quantitative precipitation forecasts provided by the simulation Liv36Ini12G4 (see Table 2) over the fourth grid were used to produce flood (discharge) forecasts at the Florence section of the Arno river (Fig. 22) by means of the TOPKAPI model (Sect. 4.2.1.; also in Todini and Ciarapica, 2002).

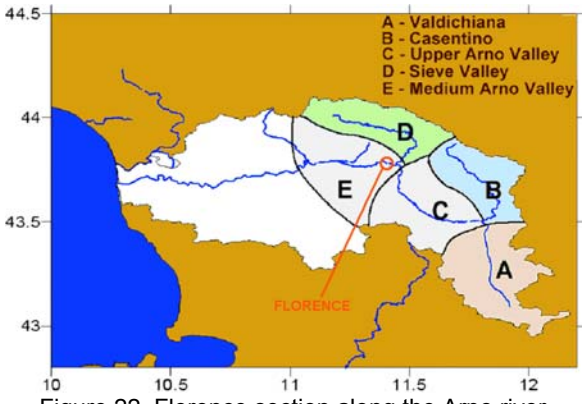

Figure 22. Florence section along the Arno river

Fig. 23 shows the flood forecasts at the Florence section, issued at different times, which assume that rainfall forecasts are not available (i.e. assuming future zero rainfall), compared with the flood forecast based on the rainfall observed at all times. The strong dependence of the flood forecasts on the initial time is apparent, and the flood warning could be provided only about three hours in advance.

Fig. 24 shows the flood forecasts at the Florence section, issued at different times, which assimilate the rainfall forecasts provided by RAMS, compared with the flood forecast based on the rainfall observed at all times. Even the earliest flood forecast, issued at 18 UTC on November 3, could lead to an accurate flood warning, i.e. about nine hours in advance, and six hours earlier with regards to the forecast issued without using QPF.

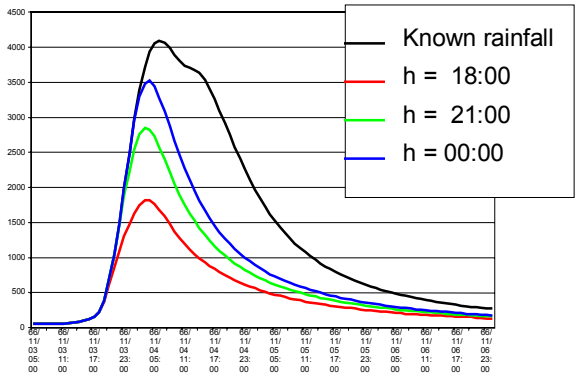

Figure 23. Flood forecasts (in m^3/s) issued at different times (18 UTC and 21 UTC on November 3 and 00 UTC on November 4) without the knowledge on future rainfall, compared to the flood wave reconstructed at Florence by means of TOPKAPI and the measured rainfall

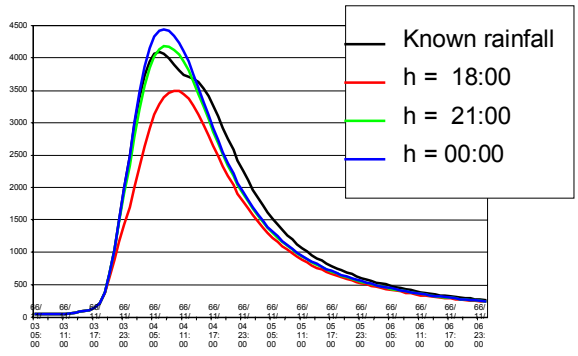

Figure 24. Flood forecasts (in m^3/s) issued at different times (18 UTC and 21 UTC on November 3 and 00 UTC on November 4) using the QPF provided by RAMS, compared to the flood wave reconstructed at Florence by means of TOPKAPI and the measured rainfall

It can be concluded that quantitative forecasts provided by RAMS could lead to a decisive improvement (i.e. anticipation) of the flood warning, when coupled to an accurate hydrological model. Thus, the QPF reveals accurate at least in the useful range for flood prediction.

4.2.3 30-year flood: October 1992

A very elongated south-westerly flux from southern north-Atlantic occurred over Mediterranean and Italy on October 30th, when a baroclinically and orographically induced low developed downwind Iberian Peninsula. Cold air penetrated far western Mediterranean during the 36 hours period and the flux became more cyclonic (warm advection). Widespread vertical velocity developed over western Mediterranean and central-northern Italy.

Such evolution is synthetically described in Fig. 25.

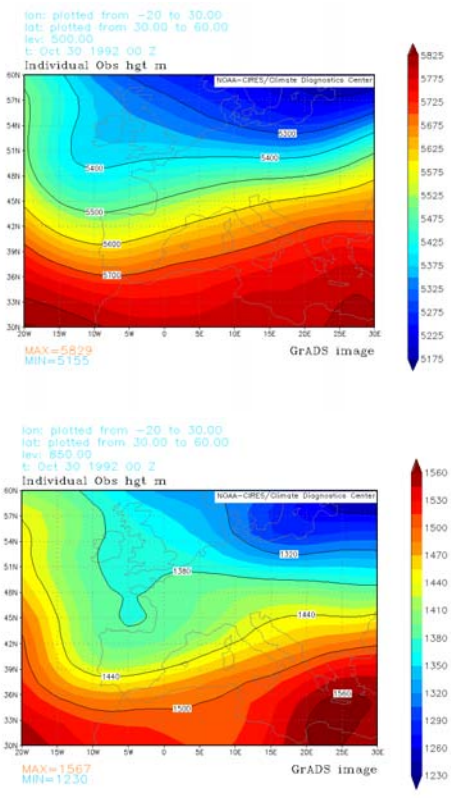

Fig. 25. 500-hPa geopotential heights at 00 UTC on October 30 (a) and October 31 (c), 1992

The precipitation which fell during the event was very extreme, reaching more than 300 mm in Tuscany (central-western Italy) and more than 500 mm in north-eastern Italy. High precipitation rates are shown over most of Arno river basin.

Five simulations were executed, testing the impact of initialization (00 UTC on October 30th and 12 UTC on October 29th), spatial horizontal resolution (finest resolution 3.2km and 1.6 km) and assimilation of sea surface temperature (climatological and observed, at resolution 1 deg Lat-Lon). Details are given in Table 3. below.

Name	G1	G2	G3	G4	V.L	sst	INI
LIV36I003G	80	16	3.2		36	CL	0
LIV36I004G	80	16	3.2	1.6	36	CL	0
LIV36SST3G	80	16	3.2		36	OB	0
LIV36SST4G	80	16	3.2	1.6	36	OB	0
LIV36SST4G_29	80	16	3.2	1.6	36	OB	-24

Table 3. Summary of features of the five RAMS simulations for the October 1992 flood (Gn = horizontal resolution of n-th grid, V.L = vertical levels, sst = sea surface temperature, CL = climatological sst, OB = observed sst, INI = initialization time: 00 = 00 UTC October 30th, -24 = 00 UTC October 29th)

The comparison of observed and predicted precipitation on the finest resolution grids for every simulation, in the period from 00 UTC on October 30th to 12 UTC on October 31st are shown in Fig. 26 (patterns), Fig. 27 (basins averages), and Fig. 28 (frequency in intensity classes).

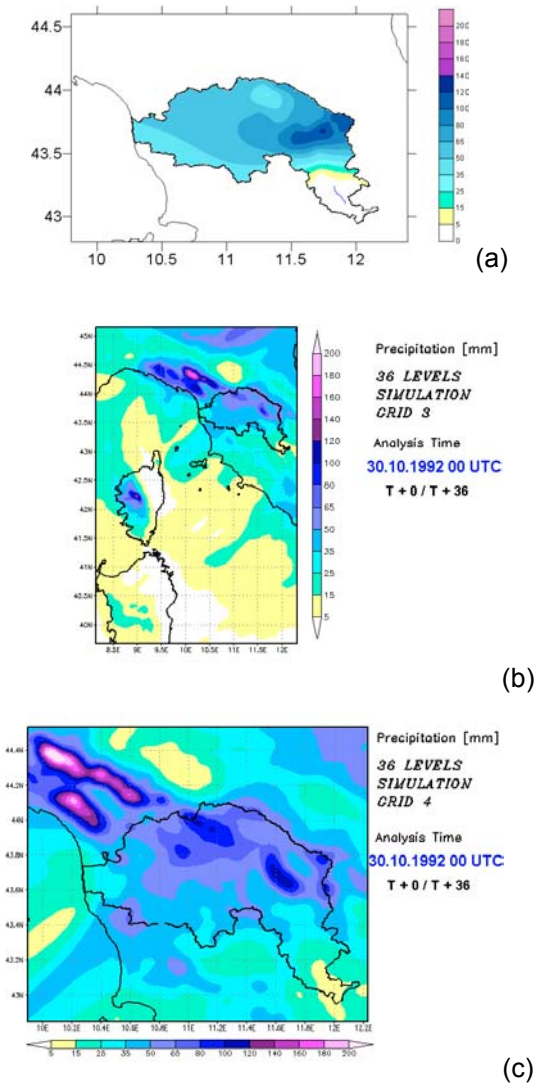

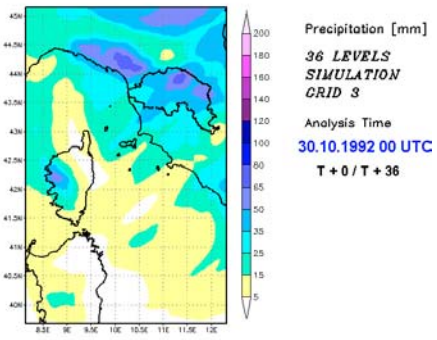

(d)

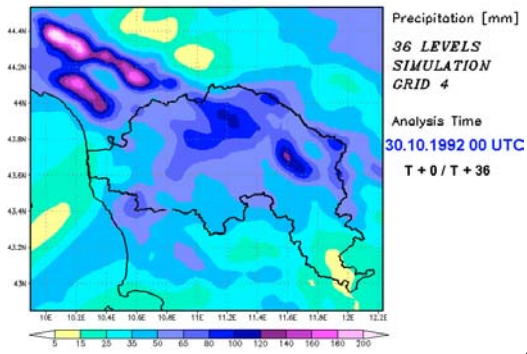

(e)

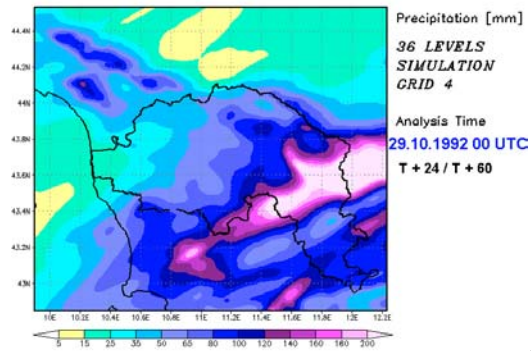

(f)

Fig. 26. Validation of RAMS QPFs: comparison of observed vs forecast rainfall distributions.between 00 UTC on October 30th 1992 and 12 UTC on October 31st 1992. (a) Observations; (b) Liv36I003G; (c) Liv36I004G; (d) Liv36SST3G; (e) Liv36SST4G; (f) LIV36SST4G_29 (see Table 3)

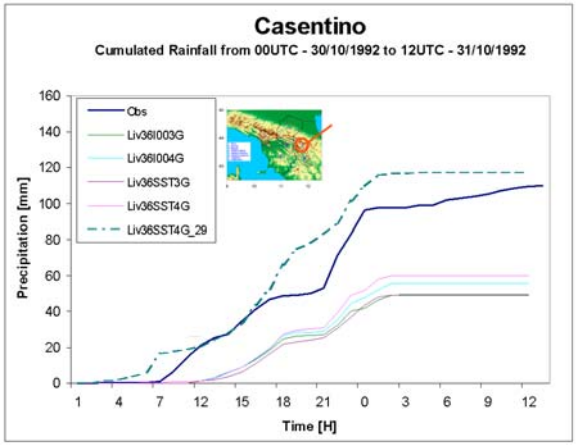

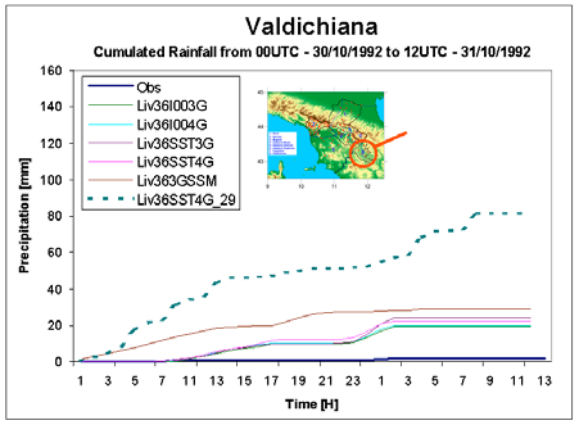

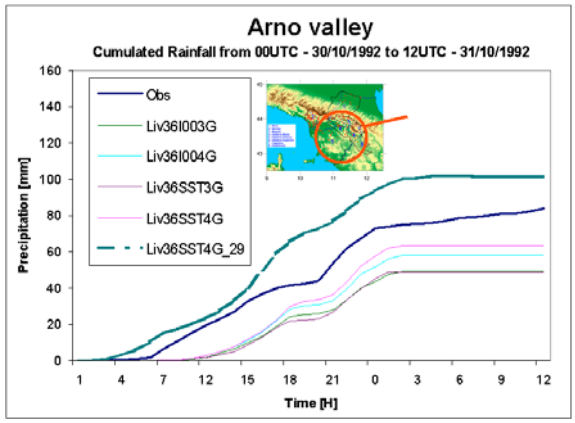

Fig. 27. Validation of RAMS QPFs: comparison of observed vs forecast average rainfall over the Casentino and Valdichiana sub-basins and the whole Arno watershed

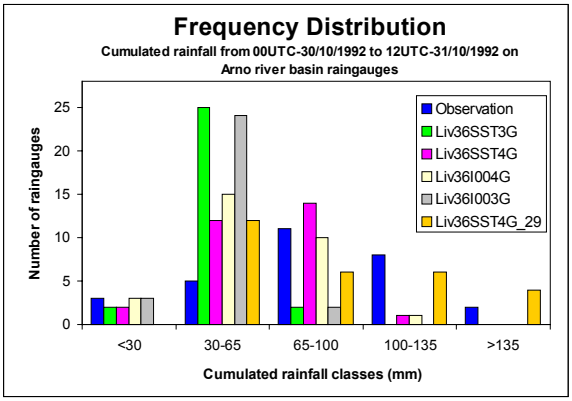

Fig. 28. Validation of RAMS QPFs: comparison of observed vs forecast distribution of rainfall, partitioned into intensity classes

The validation vs the rain gauges provides some guidance to produce accurate QPFs:

- The event was again a large scale one; no explosive cyclogenesis occurred, contrary to the 1996 event. Precipitation systems were widespread, just like the vertical velocity pattern.
- The resolution increase from 3.2 km to 1.6 km) produces significant and positive effects.
- The use of "observed" sea surface temperature instead of climatological ones, at the same spatial resolution (1 deg) produces relevant and positive effects, mostly at the finest resolution (1.2 km).
- The initialization "during" the event (00 UTC on October 30th) produced a significant underestimation, with most of missing rainfall occuring in the early simulation period (model spin-up).
- The simulation initialized at 00 UTC on October 29th, 24 before the other simulations and before the beginning of the rainstorm, produced generally very accurate forecasts in the first 18 hours of the study period (i.e. between 24 and 42 hours after its initialization), resulting sometimes in better forecasts over the whole period, but showing afterwards a relevant decay in accuracy.
- Initialization time thus shows to be critical for the success of the numerical prediction, at least during large scale rainstorm, which suggests the need to pursue either an improvement of initial conditions (e.g. by means of diabatical initialization, see Par. 4.2) or more frequent predictions (e.g. every 6-12 hours), or both.

4.3 EURAINSAT Project: Precipitation assimilation

4.3.1 The rapid update satellite precipitation estimation algorithm

The method adopted to estimate the instantaneous rain rate from satellite has been proposed by Turk et al. (2000) and it is based on the idea of blending low-Earth orbiting (LEO) microwave (SSM/I, TRMM) and geostationary (GEO) infrared data (GOES-East/West, GMS, and Meteosat) together, so to exploit the inherent advantages of each sensor.

Microwave-based imagers are suited to quantitative measurements of precipitation due to the physical connection between upwelling microwave radiation and the underlying cloud precipitation structure. On the other hand geostationary weather satellites imaging systems provide the rapid temporal update cycle needed to capture the growth and decay of precipitating clouds systems on a scale of several kilometers.

The blending of LEO and GEO measurements allows an hourly (or less) global rain rate analysis which avoids the spatial and temporal coverage gaps characteristic of swath-limited LEO data. This kind of analysis is needed for assimilation into numerical weather prediction models, especially for quantitative precipitation forecasting. In the rapid update (RU) algorithm time- and space coincident microwave and IR data are saved each time a SSM/I or TRMM pass intersects with any of the four operational geostationary satellites. The SSM/I rain rate is computed via the operational NOAA-NESDIS scheme (Ferraro, 1997) at the A scan sampling spacing (25 km) of the instrument scan operation. Once every few hours an update cycle starts and accumulate the most recent 24 hours of past coincident data.

Separate histograms of the IR temperatures and the associated microwave-based rain rates are built in a 15° grid between 60°S-60°N latitude. The grid boxes are 5° apart, providing a spatial overlap, so to assure that the statistical relationships transition smoothly from adjacent regions. To utilize only the most recent rain evolutionary history, the histograms are accumulated until the percent coverage of a given box reach a threshold (lets say 75%). The larger the percentage threshold, the longer one needs to look back in time, drawing on an increasingly earlier stage of the cloud lifecycle.

Depending on how recently a given geographical region was imaged by a MW sensor, the data used in some of the histogram boxes may be only a few hours old, whereas other regions may require more look-back time

to reach the coverage threshold. If a region has not reached the coverage threshold by the look-back time limit of 24 hours, the RU rain rate estimate is rendered (temporarily) unavailable for this region. Once the statistical relationships T_B vs rain rate are established for each 15° region, the calculation of the instantaneous rain rate for each geostationary pass is straightforwardly accomplished by simply scanning the available global lookup tables.

Figure 29. shows an example of the application of the method. The upper panel depicts the rain rate derived by means of the Ferraro (1997) algorithm for an SSM/I pass over Italy starting on 15.33 UTC on September 20th, 1999. The lower panel is the rain rate derived from METEOSAT-7 IR data, slot 34, covering data acquired from 16:00 to 16:30 UTC.

The example clearly shows that the method, due to the recent microwave pass, established a T_B-rain rate relationship suitable to follow the evolution of the cell. Indeed the duration of the MW cloud characterization is the critical point of the method, and strongly depends on the specific precipitation system.

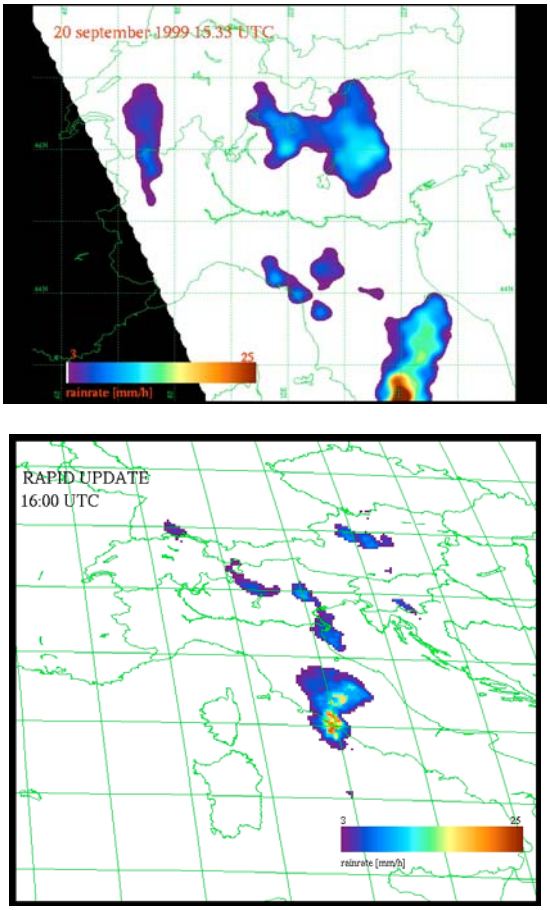

Fig. 29. a) The rain rate derived from SSM/I data and b) from the IR T_B METEOSAT-7 data by means of RU

4.3.2 Precipitation assimilation in model RAMS

In RAMS the non-resolved convective precipitation can be computed by means of the Kuo parameterisation scheme (Kuo, 1974; Molinari, 1985). From the model atmospheric variables at the base and along the column the cumulus convection module computes the water vapor convergence and then the precipitating fraction of such water. Then the module computes the convective tendencies of temperature and moisture by means of a 1-D cloud model.

In the inverted Kuo scheme the convective rainfall becomes an input, which water vapor and convective tendencies are computed from.

The impact of the observed rainfall values in the model equations is through the rates of humidity and temperature change, due to condensation and latent heat release, according to the observed rainfall rate, in each grid column where the observed convective rainfall rate is non-zero

The assimilation is performed at several time-steps during the earlier (typically six) hours of the model simulation, by weighting the observed rainfall rate with a time dependent nudging function (which can be made dependent on observation errors too).

The observed rainfall partitioning in non-resolved convective precipitation and resolved one is a tricky problem. Ancillary data (e.g. lightning) are generally difficult to be interpreted and to be managed in an operational context. In the work it is assumed that the resolved rain given by the model computation is *reliable enough* to be subtracted from the satellite total rainfall, in order to obtain the non-resolved convective quantity (negative resulting values being moved to null ones). Satellite estimation errors can be taken into account in this process by weighting the subtraction terms.

A very simple scheme of the procedure is represented in Fig. 30.

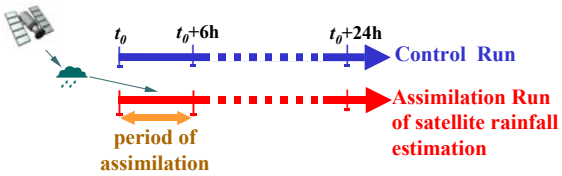

Fig. 30. Simple scheme of the rainfall assimilation procedure

4.3.3 Case study: MAP IOP2 (19-21 September 1999). Synoptic meteorology and verification of the satellite precipitation estimation

The meteorology of the case study was characterized by a deep cyclone on the Atlantic west-south-west of British Isles, with a very

elongated baroclinic front approaching western Mediterranean and France on September 19th 1999, anticipated by a southerly flow, intensifying on September 20th from interior northern Africa and producing a convergence to northern Italy and Alps from , where it converged from the seas surrounding the peninsula (south-west and south-east). The pre-frontal and frontal precipitation was widespread. The focusing and channeling of the flow, together the advection of the strongly unstable elevated mixed layer from Sahara, produced locally intense rainstorms over the main ridges of the Italian Appennines and Alps and the respective foothills, especially over the western portions of such mountains.

The patterns of geopotential at 500 hPa and Sea Level Pressure at 00 UTC on September 19th and 20th are shown in Fig. 31.

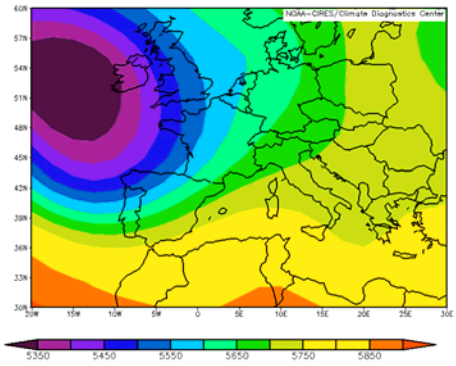

(a)

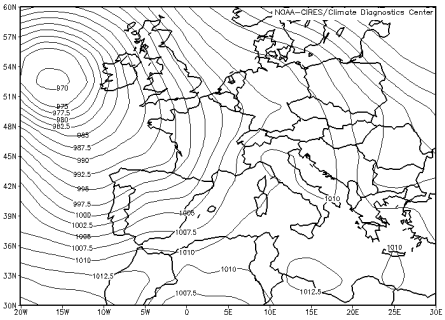

(b)

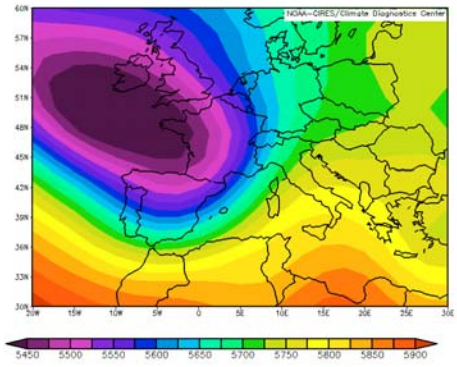

(c)

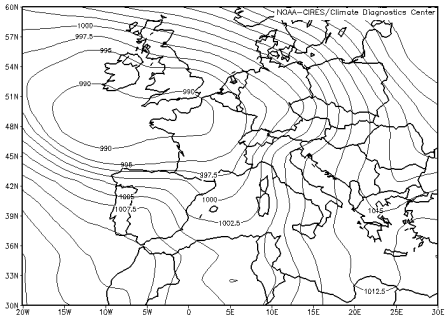

(d)

Fig. 31. Synoptic meteorology of the case study. (a) and (b): 500 hPa geopotential height and sea level pressure, respectively, at 00 UTC on September 19th; (c) and (d): 500 hPa geopotential height and sea level pressure, respectively, at 00 UTC on September 20th

On September 21st the northern expansion of a dynamical anticyclone from northern Africa produced the eastward motion of the Atlantic cyclone and the weakening of the positive vorticity over central and western Mediterranean, until on September 22nd the anticyclonic curvature of the flow, the increasing sea level pressure and mid-tropospheric geopotential marked the rapid increase of stability (not shown).

The patterns of geopotential at 500 hPa and Sea Level Pressure at 00 UTC on September 21st and 22nd are shown in Fig. 32.

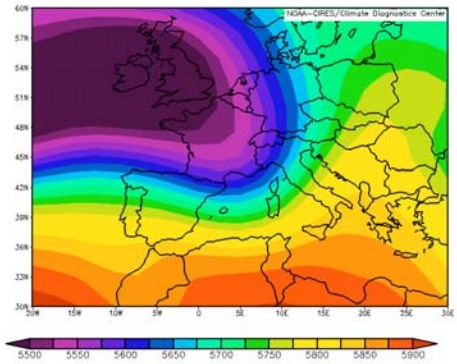

(a)

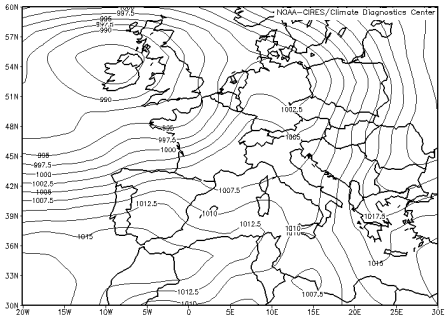

(b)

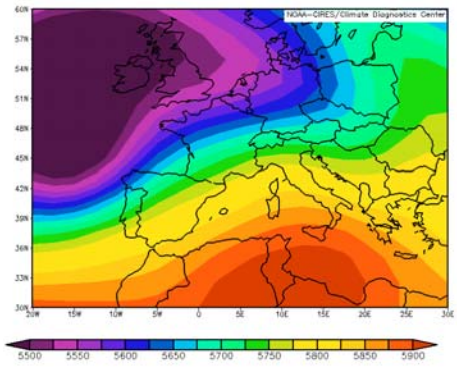

(c)

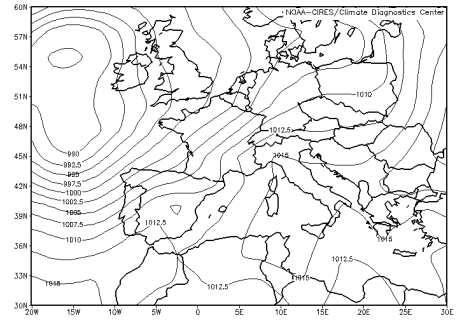

(d)

Fig. 32. Synoptic meteorology of the case study. (a) and (b): 500 hPa geopotential height and sea level pressure, respectively, at 00 UTC on September 21st; (c) and (d): 500 hPa geopotential height and sea level pressure, respectively, at 00 UTC on September 22nd

In order to validate the algorithm of rainfall estimation from satellite data (sample picture in Fig. 33), it was performed a comparison with data from a rain gauges network. A comparison with data from a network of rain gauges was performed by considering nine hydrographic basins in the area covered by the rain gauge network. The average rainfall values, computed from the data of all the rain gauges corresponding to each one of the above hydrographic basins, were compared with the corresponding average of the satellite retrieved rainfall values. An excellent agreement was found for four out of the nine analyzed basins.

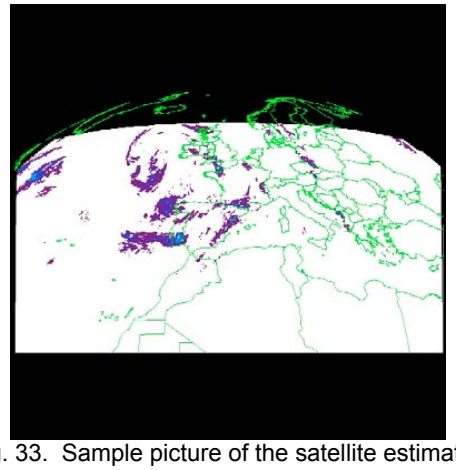

Fig. 33. Sample picture of the satellite estimated rainfall

In such basins both the temporal phase of the event and the total cumulated rainfall are well retrieved by the algorithm. For one of the four basins an excellent accordance is shown in the temporal phase, but a significant discrepancy in the cumulated rainfall.

For the three other basins, we have an insufficient time alignment and strong discrepancies in the cumulated rainfall.

In Fig. 34 (a) and (b) it is reported the time evolution of the observed and satellite estimated cumulated rainfall for the Valdarno Inferiore basin, where an excellent agreement is shown, in the period from 00 UTC on September 20th to 00 UTC on September 22nd.

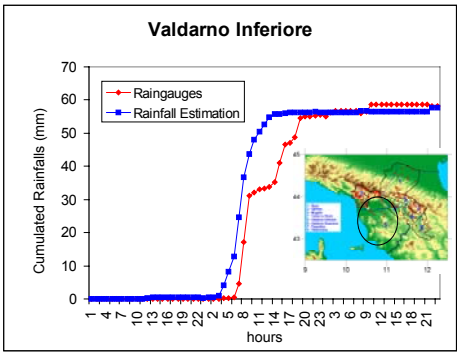

(a)

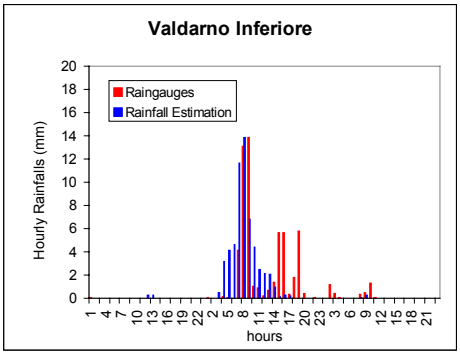

(b)

Fig. 34. Validation of the satellite rainfall estimation for the Valdarno Inferiore basin in the period from 00 UTC on September 20th to 00 UTC on September 22nd. (a): time evolution of cumulated rainfall; (b): time evolution of hourly rainfall

The performance of the satellite estimation algorithm appears to be excellent, in this case study, for the coastal areas where orography is particularly smooth, while it shows large deficiencies (not shown) for steep orography areas, mainly due to known problems affecting the microwave rainfall retrievals over the land surface and the lack of orographical corrections in both the microwave and infrared modules.

Model RAMS was run for 48 hours since 00 UT on September 20th over a large domain covering central-western Mediterranean and Europe at 20 km spatial horizontal resolution. Fig. 35 shows the domain with a sample hourly precipitation field superimposed.

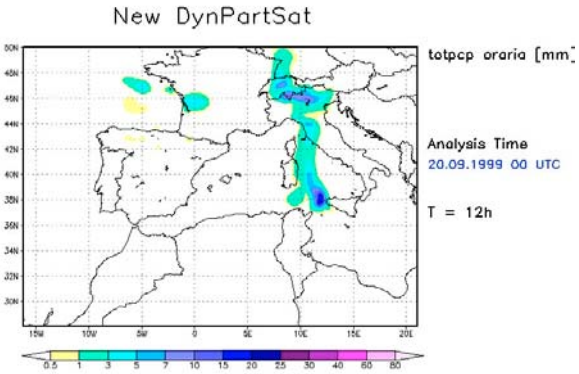

Fig. 35. Domain of model RAMS and sample hourly precipitation field after 12 hours of simulation

Two simulations were executed: a *control run* without assimilation of the satellite estimated rainfall, and a *dynamical satellite assimilation run* in which the assimilation is performed.

Fig. 36 shows the basins for which the rainfall forecasts produced by the two simulations executed with RAMS model are validated.

Fig. 37 shows the results of the validation for four basins.

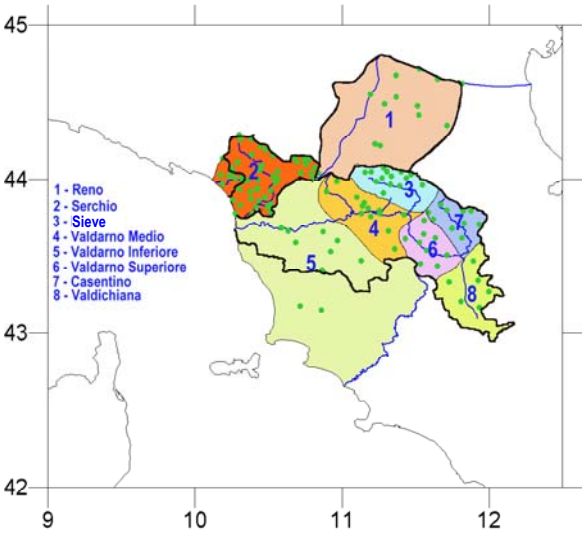

Fig. 36. Hydrographic basins used for the validation of the rainfall forecasts produced by the RAMS model

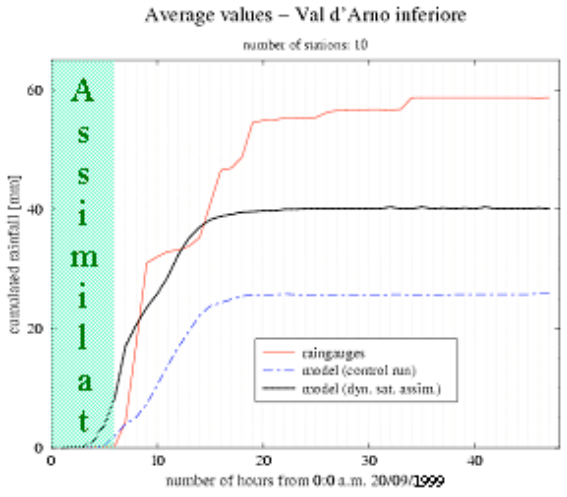

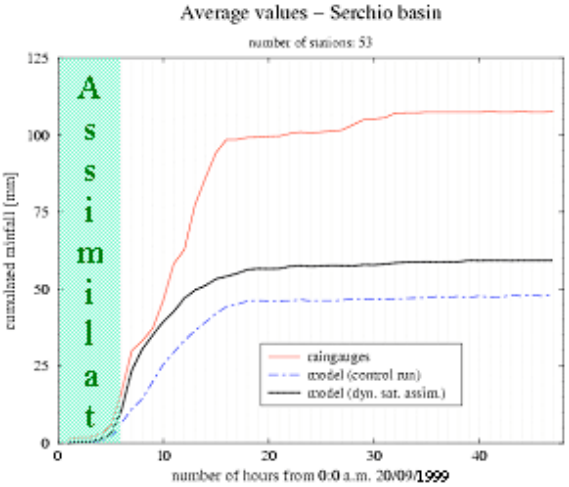

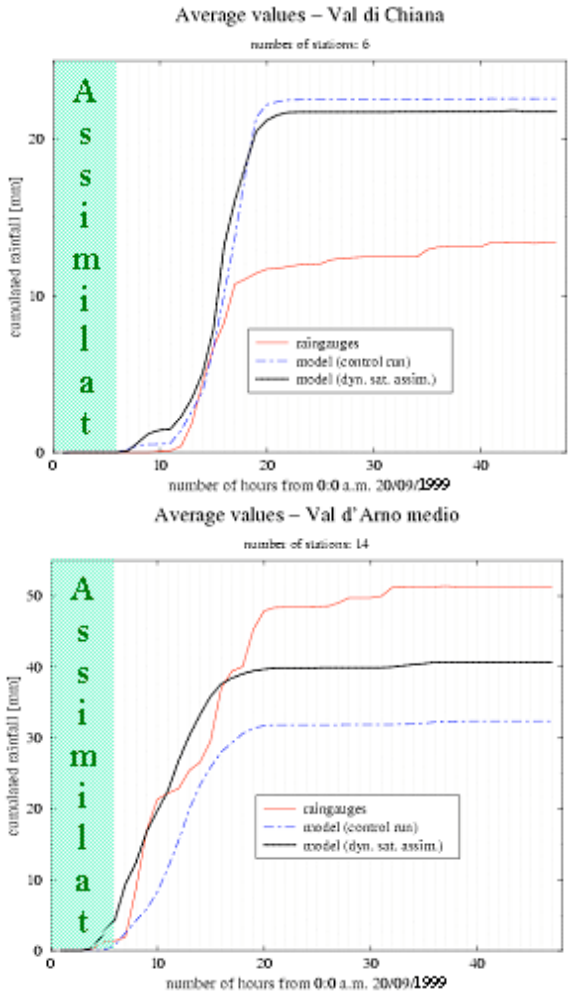

Fig. 37. Validation of RAMS QPFs: comparison of observed vs forecast average rainfall over the Valdarno Inferiore, Serchio, ValdiChiana and Valdarno Medio sub-basins

The main results of satellite precipitation assimilation into RAMS can be summarized in the following points:

- The convective rainfall assimilation technique correctly converges.
- The impact of convective rainfall assimilation on simulations started *during* convection events is relevant.
- Assimilation improves spin-up phases and rainfall forecasts up to several hours.
- Positive effects of assimilation are generally found both on the Kuo - parametrized and the resolved parts of the rainfall forecasted by the model.
- The improvements are apparent several hours after the end of the assimilation period.

Other experiments are anyway necessary to evaluate the impact of the precipitation assimilation in different synoptic and mesoscale meteorological conditions .

5. DISCUSSION AND CONCLUSIONS

This work describes the recent improvements in a regional meteorological prediction system based on model RAMS, mainly aimed at quantitative precipitation forecasting.

The sensitivity of the prediction quality to several key components is analyzed, comprising horizontal and vertical resolution, initialization time, quality of the assimilated sea surface temperature and precipitation assimilation.

Special emphasis is given to the low cost high-performance computer system, which allows to pursue the improvements while preserving operational simulation times, and to the coupling to a hydrological forecasting system in view of early flood warnings. The improvement of such warnings also provide some more information on the quality of the atmospheric model forecasts.

Some guidance is derived as regards the production of accurate quantitative precipitation forecasts, which constitute a sound basis for future work and developments.

6. REFERENCES

Abbott, M.B. et al., 1986a: An introduction to the European Hydrological System - Système Hydrologique Européen, "SHE", 1: History and philosophy of a physically-based, distributed modelling system. *J. Hydrol.,* **87**, 45-59.

Abbott, M.B. et al., 1986b: An introduction to the European Hydrological System - Système Hydrologique Européen, "SHE", 2: Structure of physically-based, distributed modelling system. *J. Hydrol.*, **87**, 61-77.

Barnes H.H., 1967: Roughness Characteristics of Natural Channels. *Geological Survey Water-Supply Paper 1849*. US Gov. Printing Office, Washington.

Beven, K.J. and Kirkby, M.J., 1979: A physically based, variable contributing area model of basin hydrology. *Hydrol. Scien.*, **24**, 1-3.

Burnash, R.J.C., Ferral, R.L. & Mc Guire, R.A.,1973: A General Streamflow Simulation System - Conceptual Modelling for Digital

Computers, *Report by the Joint Federal State River Forecasts Center*, Sacramento.

Chow Ven Te, 1959: Open Channel Hydraulics. *McGraw-Hill Book Company, Inc.*, Kogakusha Company, Ltd., Tokyo.

Ciarapica L., Todini E., 2002: TOPKAPI: a model for the representation of the rainfall-runoff process at different scales. *Hydrological Processes*, **16(2)**, 207-229.

Ferraro, R. R., 1997: Special sensor microwave imager derived global rainfall estimates for climatological applications, *J. Geophys. Res.*, **102**, **D14**, 16715-16735.

Kalnay, E. and Coauthors, 1996: The NCEP/NCAR Reanalysis 40-year Project. *Bull. Amer. Meteor. Soc.*, **77**, 437-471.

Kuo, H. L., 1974: Further studies of the influence of cumulus convection on large-scale flow. *J. Atmos. Sci.*, **31**, pp 1232-1240.

Meneguzzo, F., Menduni, G., Maracchi, G., Zipoli, G., Gozzini, B., Grifoni, D., Messeri, G., Pasqui, M., Rossi, M., and C.J. Tremback, 2002: Explicit forecasting of precipitation: sensitivity of model RAMS to surface features, microphysics, convection, resolution. In: *Mediterranean Storms. 3rd Plinius Conference 2001*. Ed. by: R. Deidda, A. Mugnai, F. Siccardi. GNDCI Publ. N. 2560, ISBN 88-8080-031-0, 79-84.

Mission Research Corporation (MRC)/*ASTER Division, 2000: RAMS. The Regional Atmospheric Modeling System. Technical Description. [Available at http://www.aster.com].

Molinari, J., 1985: A general form of Kuo's cumulus parameterisation, *Mon. Wea. Rev.*, **113**, pp 1411-1416.

Moore, R.J. and Clarke, R.T., 1981: The probability-distributed principle and runoff production at point and basin scales. *Hydrol. Sci. J.*, **30(2)**, 273-297.

Pielke, R. A. & Coauthors, 1992: A comprehensive meteorological modeling system-RAMS. *Meteor. Atmos. Phys.*, **49**, 69–91.

Rockwood, D.M., 1961: Columbia Streamflow Routing by Computer. *Trans. ASCE*, Paper n. 3119.

Rockwood, D.M. and Nelson, M.L., 1966: Computer application to Streamflow Synthesis and Reservoir regulation. *Proc. IV Int. Conference on Irrigation and Drainage*.

Rockwood, D.M et al., 1972: User Manual for COSSARR Model, US Army Engineering Division North Pacific. Portland Oregon.

Todini, E., 1995: New trends in modelling soil processes from hillslope to GCM scales, in The Role of Water and the Hydrological Cycle. In: *Oliver, H. R. and Oliver, S. A. Global Change NATO ASI Series, Series I: Global Environmental Change*, **31**, 317-347.

Todini E., 1996: The ARNO Rainfall-Runoff model, *J. Hydrol.*, **175**, 339-382.

Todini, E. and Ciarapica L., 2002: The TOPKAPI model. In Mathematical Models of Large Watershed Hydrology. V. P. Singh, D. K. Frevert and S. P. Meyer (eds.), *Water Resources Publications*, Littleton, Colorado, **Chapter 12**, 471-506.

Tremback, C. J., 1990: Numerical simulation of a mesoscale convective complex: model development and numerical results. Ph.D. dissertation, *Atmos. Sci. Paper No. 465*, Colorado State University, Dept. of Atmospheric Science, Fort Collins, CO 80523.

Turk, F. J., G. D. Rohaly, J. Hawkins E. A. Smith, F. S. Marzano, A. Mugnai, and V. Levizzani, 2000: Meteorological applications of precipitation estimation from combined SSM/I TRMM and infrared geostationary satellite data, In *Microwave Radiometry and Remote Sensing of the Earth's Surface and Atmosphere*, P. Pampaloni and S. Paloscia Eds., VSP Int. Sci. Publ., 353-363.

Walko, R. L., W. R. Cotton, M. P. Meyers, and J. Y. Harrington, 1995: New RAMS cloud microphysics parameterization. Part I: The single-moment scheme. *Atmos. Res.,* **38**, 29–62.

Walko, R. L., & Coauthors, 2000: Coupled atmosphere–biophysics–hydrology models for environmental modeling. *J. Appl. Meteor.,* **39,** 931–944.

Wilks, D.S., 1995: Statistical methods in the atmospheric sciences: an introduction. *Academic Press*, 464 pp.

Zhao, R.J., 1977. Flood forecasting method for humid regions of China. *East China College of Hydraulic Engineering*, Nanjing, China.